Beam-normal single spin asymmetry in elastic electron scattering off 28Si and 90Zr

Esser, A.; Thiel, M.; Achenbach, P.; Aulenbacher, K.; Aulenbacher, S.; Baunack, S.; Bosnar, D.; Caiazza, S.; Christmann, M.; Dehn, M.; ...

Source / Izvornik: **Physics Letters B, 2020, 808**

Journal article, Published version
Rad u časopisu, Objavljena verzija rada (izdavačev PDF)

https://doi.org/10.1016/j.physletb.2020.135664

Permanent link / Trajna poveznica: https://urn.nsk.hr/urn:nbn:hr:217:237078

Physics Letters B 808 (2020) 135664

Contents lists available at ScienceDirect

Physics Letters B

www.elsevier.com/locate/physletb

Beam-normal single spin asymmetry in elastic electron scattering off ^{28}Si and ^{90}Zr

A. Esser [a,*], M. Thiel [a], P. Achenbach [a], K. Aulenbacher [a], S. Aulenbacher [a], S. Baunack [a], D. Bosnar [b], S. Caiazza [a], M. Christmann [a], M. Dehn [a], M.O. Distler [a], L. Doria [a], P. Eckert [a], M. Gorchtein [a], P. Gülker [a], P. Herrmann [a], M. Hoek [a], S. Kegel [a], P. Klag [a], H.-J. Kreidel [a], M. Littich [a], S. Lunkenheimer [a], F.E. Maas [a], M. Makek [b], H. Merkel [a], M. Mihovilovič [a,c], J. Müller [a], U. Müller [a], J. Pochodzalla [a], B.S. Schlimme [a], R. Spreckels [a], V. Tioukine [a], C. Sfienti [a]

[a] Institut für Kernphysik, Johannes Gutenberg-Universität Mainz, D-55099 Mainz, Germany
[b] Department of Physics, Faculty of Science, University of Zagreb, 10000 Zagreb, Croatia
[c] Jožef Stefan Institute, SI-1000 Ljubljana, Slovenia

ARTICLE INFO

Article history:
Received 30 April 2020
Received in revised form 27 July 2020
Accepted 27 July 2020
Available online 30 July 2020
Editor: D.F. Geesaman

Keywords:
Transverse asymmetry
Elastic scattering
Polarized beam
Multi-photon exchange

ABSTRACT

We report on a new measurement of the beam-normal single spin asymmetry A_n in the elastic scattering of 570 MeV transversely polarized electrons off ^{28}Si and ^{90}Zr at $Q^2 = 0.04$ GeV$^2/c^2$. The studied kinematics allow for a comprehensive comparison with former results on ^{12}C. No significant mass dependence of the beam-normal single spin asymmetry is observed in the mass regime from ^{12}C to ^{90}Zr.

1. Beam-normal single spin asymmetry

Measurement of parity violation in weak interactions is a well established experimental technique in atomic, particle and nuclear physics. Over the past 30 years, precision experiments have probed hadron [1–6] and nuclear structure [7] and new proposals have recently been put forward that will considerably improve our understanding of the electroweak interaction and will allow us to explore physics beyond the standard model [8–10].

The interpretation of these future measurements requires theoretical predictions with uncertainties below those of the experiments. To that end it is mandatory to go beyond the one-photon exchange approximation and include higher-order corrections (such as γZ- [11], γW-, [12] or $\gamma\gamma$-box graphs [13]) in the calculations.

The measurement of observables sensitive to two-photon exchange processes is essential to benchmark such higher-order calculations.

For this purpose the beam-normal single spin asymmetry (the so-called transverse asymmetry) A_n in polarized electron-nucleus scattering is an ideal candidate. Since A_n is a parity conserving asymmetry, arising from the interference of one- and two (or more)-photon exchange amplitudes, it gives direct access to the imaginary part of the two-photon exchange process.

A_n can be observed when the polarization vector $\vec{P}_e$ of the electrons is aligned parallel or antiparallel to the normal vector $\hat{n} = (\vec{k} \times \vec{k}')/|\vec{k} \times \vec{k}'|$ of the scattering plane, where $\vec{k}$ ($\vec{k}'$) are the three-momenta of the incident (scattered) electrons. The measured beam-normal single spin asymmetry in the two-photon approximation can be expressed as

$$A_n = \frac{\sigma^{\uparrow} - \sigma^{\downarrow}}{\sigma^{\uparrow} + \sigma^{\downarrow}} = \frac{2\,\mathrm{Im}\left(\mathcal{M}_{\gamma}^{*} \cdot \mathcal{M}_{\gamma\gamma}\right)}{|\mathcal{M}_{\gamma}|^2}, \tag{1}$$

where $\sigma^{\uparrow}$ ($\sigma^{\downarrow}$) denotes the cross section for electrons with spin parallel (antiparallel) to the normal vector $\hat{n}$. In Eq. (1), $\mathrm{Im}(\mathcal{M}_{\gamma}^{*} \cdot$

* Corresponding author.
E-mail address: esser@uni-mainz.de (A. Esser).

https://doi.org/10.1016/j.physletb.2020.135664

$\mathcal{M}_{\gamma\gamma}$) denotes the imaginary part of the one- and two-photon exchange amplitudes $\mathcal{M}_{\gamma}$ and $\mathcal{M}_{\gamma\gamma}$ [14], respectively. The measured asymmetry is related to A_n by

$$A_{exp} = A_n \vec{P}_e \cdot \hat{n}. \quad (2)$$

The transverse asymmetry roughly scales as $\frac{m_e}{E}\alpha_{em}$, with m_e the electron mass, E the beam energy, and α_{em} the electromagnetic coupling constant [15]. Asymmetries as small as 10^{-5} to 10^{-6} are therefore expected for beam energies of several hundred MeV. This makes the experiments particularly challenging, as statistical and systematic errors in the measurement need to be kept well below 10^{-6}.

The theoretical treatment of A_n is nontrivial as well since the absorptive part of the two-photon exchange amplitude has to be related to the sum of all possible physical (on-mass-shell) intermediate states. While several approaches are available to calculate the transverse asymmetry for the reaction $p\,(e,e')\,p$ [15–18], only two different calculations, exploiting different ansatzes, allow for an extension to nuclei with $Z \geq 2$. Cooper and Horowitz [19] are numerically solving the Dirac equation to calculate Coulomb distortion effects. To do so, they assume that only the ground state contributes, especially with increasing Z. In contrast, Gorchtein and Horowitz [20], following the approach by Afanasev and Merenkov [17,18], include a full range of intermediate states (elastic and inelastic) but limit their calculation to the very low four-momentum transfer region ($m_e c \ll Q \ll E/c$). In this model the asymmetry can be written as:

$$A_n \sim C_0 \log\left(\frac{Q^2}{m_e^2 c^2}\right) \frac{F_{Compton}(Q^2)}{F_{ch}(Q^2)}, \quad (3)$$

with C_0 being the energy-weighted integral over the total photoabsorption cross section. It can be model-independently obtained from the optical theorem and it depends on mass number A and charge number Z of the target nucleus. The last term in Eq. (3), the ratio of Compton to charge form factor, allows the model to be generalized to nuclear targets. For this, the value of the Compton slope parameter B, given in the exponential form of the Compton form factor ($\exp(-BQ^2)$), needs to be determined. The available high-energy Compton scattering data on ^{1}H and ^{4}He (see [20] and references therein) suggest an approximate independence of $F_{Compton}(Q^2)/F_{ch}(Q^2)$ from the target nucleus, using

$$B \approx \frac{R_{Ch}^2}{6} + \frac{4}{(\mathrm{GeV}^2/c^2)} \quad (4)$$

for the Compton slope parameter, with R_{Ch} being the charge radius of the nucleus. This estimate has been adopted as a reference value for the calculation in [20]. While at low momentum transfer the Q^2 dependence of A_n is dominated by the logarithmic term, at larger Q^2 the knowledge of the exact value of the Compton slope parameter B becomes more important.

2. Previous studies

So far, the transverse asymmetry at forward angles ($\theta < 6°$) has been measured at the Thomas Jefferson National Accelerator Facility (JLab) for ^{1}H, ^{4}He, ^{12}C, and ^{208}Pb [21]. Although the data span the entire nuclear chart, a systematic interpretation in terms of Q^2, Z, and E dependence is hindered by the different kinematics of each measurement. A comparison to available theoretical calculations [17,18,20] shows a good agreement for light nuclei, with the corresponding asymmetry being dominated by inelastic contributions. At the same time, a striking disagreement in the case of ^{208}Pb was observed: this may indicate the inadequacy of the two-photon exchange (TPE) approximation in [20] given that the expansion parameter of the perturbation theory is not small ($Z\alpha \sim 1$). If this were the case, the breakdown of the TPE model of Ref. [20] should already become noticeable with intermediate heavy nuclei, thus calling for a systematic study in this mass range.

As a first step, the Q^2 dependence of A_n for carbon has been measured in the range between 0.02 GeV$^2/c^2$ and 0.05 GeV$^2/c^2$. The obtained results show a reasonable agreement with the existing theoretical calculation [22]. The deviations from the theoretical description have been related to the assumption of the dominance of the $\log(Q^2/m_e^2c^2)$ term and the independence of $F_{Compton}(Q^2)/F_{ch}(Q^2)$ from the target nucleus. The result emphasizes that the Q^2 behavior of the asymmetry cannot be treated independently of the target nucleus. Even larger discrepancies could be expected for heavier nuclei.

Therefore, a new experiment has been performed with the same setup and within the same four-momentum transfer range with the aim of investigating heavier target materials such as ^{28}Si and ^{90}Zr.

3. New measurements

These experiments were carried out at the Mainz Microtron MAMI [23] using the spectrometer setup of the A1 Collaboration [24], a well established facility for high resolution spectroscopy in electron scattering experiments. To allow for a comparison with previous results, the data were taken with the same kinematics as reported in [22]. Minor adjustments due to the different target materials led to slightly different spectrometer angles and Q^2 values as given in Table 1. In order to study the transverse asymmetry A_n, the A1 setup was slightly modified by inserting additional fused-silica Cherenkov detectors in the focal plane of the two high-resolution spectrometers A and B. These detectors are capable of handling high data rates and they allow to separate elastic from inelastic events. Corresponding to the different focal plane geometries of spectrometers A and B, the size of the fused-silica bars were chosen to be $(300 \times 70 \times 10)$ mm^3 and $(100 \times 70 \times 10)$ mm^3, respectively. The fused-silica detectors were oriented at 45° with respect to the direction of the elastically scattered electrons in the spectrometer. The produced Cherenkov light was collected by photomultiplier tubes (PMTs) with fused-silica windows.

In the MAMI beam source, the primary electrons were produced by illuminating a strained GaAs/GaAsP super lattice photocathode with circularly polarized laser light [25,26]. In order to measure the transverse asymmetry with the described spectrometer setup, the polarization vector of the emitted – longitudinally polarized – electrons had to be aligned vertically in order to be perpendicular to the scattering plane. In this two-step process, the longitudinal spin is first rotated to transverse orientation in the horizontal plane using a Wien filter [27]. Secondly, the polarization vector is rotated to the vertical orientation using a pair of solenoids. The polarization was verified to be solely vertical to within 1% using a Mott polarimeter [28] located downstream of the 3.5 MeV injector linac and a Møller polarimeter [29] close to the interaction point in the spectrometer hall. Details on this procedure can be found in [30]. Measurements with both polarimeters determined the absolute degree of polarization. During each experimental campaign the degree of polarization was monitored by frequent measurements with the Mott polarimeter. The full range of variation of the absolute degree of polarization throughout the different measurements was between 78.2% and 83.6%.

The polarized electron beam had an energy of 570 MeV and an intensity of 20 μA. It was impinging on a 1.17 g/cm^2 (1.11 g/cm^2) ^{28}Si (^{90}Zr) target with an isotopic purity of 99.9% (97.7%). Both targets needed to be cooled during the measurement to avoid a variation of their densities due to melting. For this purpose a custom-

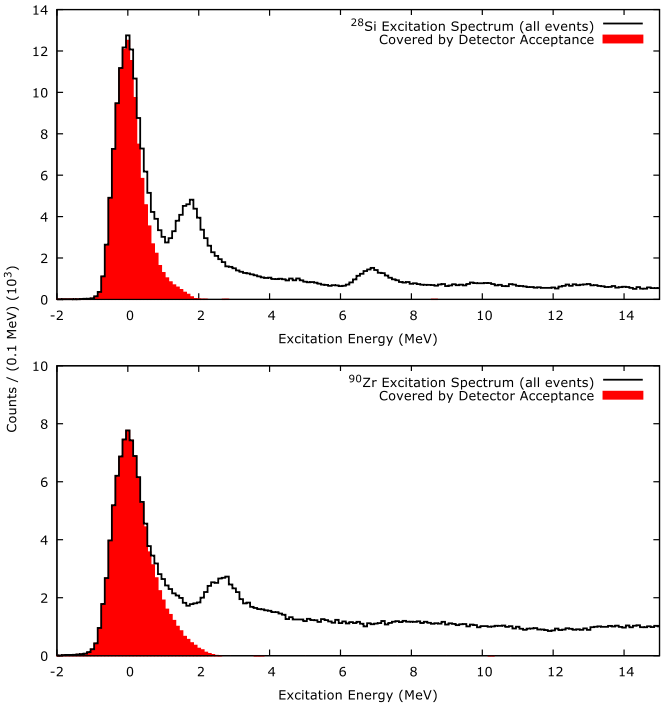

Fig. 1. The excitation energy spectra of ^{28}Si (top panel) and ^{90}Zr (bottom panel) show the acceptance of the spectrometer without (black line) and with (filled areas) a cut on the Cherenkov detector. By changing the magnetic field of the spectrometer the elastic peak was aligned with the position of the Cherenkov detector.

made cooling frame was constructed. The targets, with an active area of 10 mm × 10 mm each, were attached to a copper support structure, which was mounted on an outer aluminum frame. In this outer frame a mixture of water and ethanol was circulated at a stabilized temperature $T_{\mathrm{circ}} = 0.5\,^{\circ}\mathrm{C}$. To spread the heat load of the point-like beam spot, the electron beam was rastered over an area of 4 mm × 4 mm. For this purpose wobbler magnets running synchronized to the power grid with a harmonic frequency of 2000 (2050) Hz in horizontal (vertical) direction have been used.

The fused-silica detectors had to be positioned in such a way that they completely covered the elastic line while minimizing the contribution of the excited states. Given that the momentum acceptance of the fused-silica bar covered only part of the whole spectrometer acceptance, the magnetic field of the spectrometer was set such that the elastic peak appeared at the position of the Cherenkov detector. This geometrical adjustment was complicated by the small distance between the elastic peak and the first excited state of only $\Delta E \approx 1.8$ MeV for both targets. To verify the exact placement of the fused-silica detectors, a low beam current of $I \approx 20$ nA was used. In this mode, the events were processed individually by a conventional data acquisition system measuring timing and charge of the PMT pulses in parallel with the other detectors in the spectrometers. The accurate position information obtained from a set of drift chambers allowed to match the position of the elastic line of the scattered electrons to the Cherenkov detectors. The resulting detector coverage is illustrated in Fig. 1.

In the integrating mode of data taking used for the asymmetry measurements, the beam current was raised to 20 µA. The current produced by each detector PMT was integrated over 20 ms long periods (so-called polarization-state windows) synchronized to the power-grid frequency. These windows were arranged in a random sequence of quadruples with the orientation of the electron beam polarization being either ↑↓↓↑ or ↓↑↑↓. The polarization state was reversed by setting the high voltage of a fast Pockels cell in the optical system of the polarized electron source. A 80 µs time window between the polarization-state windows allowed for the high voltage of the Pockels cell to be switched. The integrated PMT signal for each polarization-state window was then digitized and recorded.

In order to identify and reduce polarity correlated instrumental asymmetries, several methods have been applied to reverse the sign of the measured asymmetry. Besides reversing the polarization vector orientation between the measuring gates, the differential electrical signal switching the polarity at the beam source was reversed every five minutes. Additionally, a half-wave plate in the optical system at the beam source [31] was used to reverse the beam polarity on a time scale of 24 hours.

Fluctuations of beam parameters, such as current (I), energy (E), horizontal and vertical position (x and y), and horizontal and vertical slope (x' and y'), are partly correlated to the reversal of the polarization vector orientation. This can introduce instrumental asymmetries. Therefore, it is of utmost importance to constantly control these beam parameters. They have been measured by a set of monitors: PIMO (Phase and Intensity MOnitor), ENMO (ENergy MOnitor), and XYMO (XY MOnitor). Their signals were used in a dedicated stabilization system to minimize polarity correlated beam fluctuations (see Fig. 2) [31,32].

In parallel, the output signals of the monitors were acquired in the same way as the detector signals to correct for instrumental asymmetries in the offline analysis.

4. Data analysis

As a first step, all acquired values were corrected for fluctuations in the integration gate length. Secondly, after the detector signals were offset-corrected, the raw asymmetry could be calculated:

$$A_{\mathrm{raw}} = \frac{N_{\mathrm{e}}^{\uparrow} - N_{\mathrm{e}}^{\downarrow}}{N_{\mathrm{e}}^{\uparrow} + N_{\mathrm{e}}^{\downarrow}}, \tag{5}$$

where $N_{\mathrm{e}}^{\uparrow(\downarrow)}$ is the corrected detector signal. Assuming a linear behavior of detectors and data acquisition, $N_{\mathrm{e}}^{\uparrow(\downarrow)}$ is proportional to the number of elastically scattered electrons for each polarization state. To determine the experimental asymmetry

$$A_{\mathrm{exp}} = A_{\mathrm{raw}} - c_1 A_{\mathrm{I}} - c_2 \Delta x - c_3 \Delta y - \\ - c_4 \Delta x' - c_5 \Delta y' - c_6 \Delta E, \tag{6}$$

the raw asymmetry needs to be corrected for instrumental asymmetries. Here, c_i $(i = 1, \ldots, 6)$ are the correction factors, A_{I} is the beam current asymmetry, Δx and Δy are the polarity correlated differences of the horizontal and vertical beam position, $\Delta x'$ and $\Delta y'$ are the differences in beam angle, and ΔE is the difference in beam energy. The physical parameters of the beam have to be extracted from the beam monitor data and the correction factors c_i need to be determined. Due to the beam stabilization system, the helicity-correlated changes of the beam parameters were small but not negligible.

For the calibration of the beam monitors, dedicated runs were performed. The PIMO signal together with the PMT gain was automatically calibrated in special runs, which have been performed approximately every three hours. For these special runs the beam current was ramped up in steps of 0.25 µA from 17.5 µA to 22.5 µA, covering the nominal beam current setting. The integrated PMT signal was calibrated against the beam current allowing for the extraction of an individual offset for every PMT. This procedure also allowed to constantly check the linearity of the PMT responses and to monitor any gain variations. A precise calibration of the PIMO was also essential for the calibration of XYMOs and ENMO, since their signals scale with the beam current.

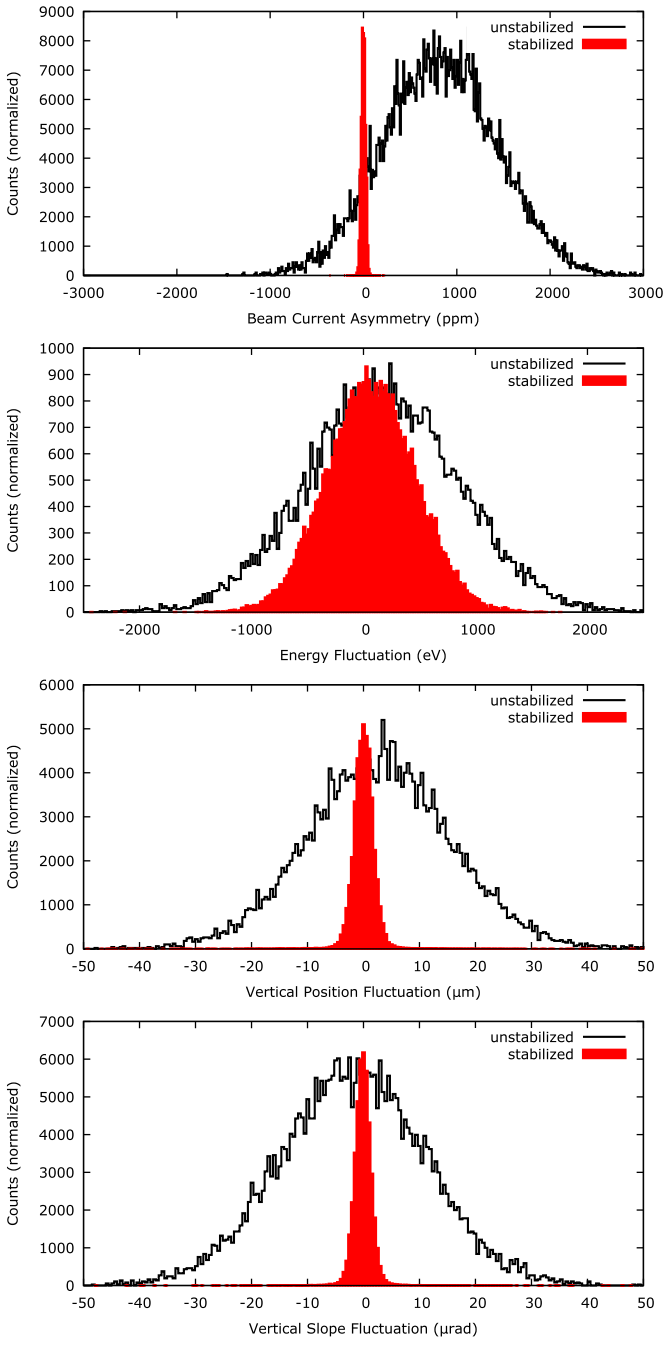

Fig. 2. Comparison between the beam parameters observed in a run with beam stabilization off (black) and with beam stabilization on (red).

For the XYMO calibrations, the beam was slowly rastered over wire targets with known wire positions. For the ENMO calibration an electronic, polarity-correlated signal corresponding to a defined energy variation was superimposed on the raw energy signal. XYMOs and ENMO were calibrated once per experimental campaign.

While the correction factor c_1 for the beam current asymmetry was set to a fixed value of 1, the other factors c_i were obtained by an iterative optimization procedure. Its purpose was to minimize the dependence of the corrected asymmetry A_{exp} on the polarity correlated differences of the beam parameters. Therefore, the analysis was run repeatedly, and each time the resulting experimental asymmetry (A_{exp}) was linearly fitted against the polarity correlated difference of each beam parameter. Then all correction factors were modified simultaneously in small increments to counteract this dependence. This procedure was repeated until a minimal dependence was achieved. 0.01% of all events were excluded from the analysis due to either a wrong gate-length signal or the beam current being outwith the calibration range.

5. Results

The results obtained for A_{n} together with their uncertainties are shown in Table 1. Large beam fluctuations and short running time affects the ^{90}Zr result that exhibits larger statistical and systematic errors compared to both the ^{28}Si measurement and our former ^{12}C result [22].

The systematic errors consist of a set of contributions arising from different sources. The contributions introduced by fluctuations of position, angle, and energy of the beam were determined by varying the correction factors independently by $\pm 25\%$ and calculating the maximum change in the resulting asymmetry. The threshold for excluding events with short drops in the beam current was varied over a wide range around the lower boundary of the beam current calibration range to evaluate the influence of this threshold on the resulting transverse asymmetry. A negligible effect of no more than 0.03 ppm was found (ΔCurrentDrop in Table 1), which contributed to the systematic uncertainty.

The current and gate-length asymmetry was measured for every event. In order to estimate a conservative systematic uncertainty, the statistical error of their mean asymmetry was added to the systematic uncertainty (ΔA_{I} and ΔA_{GL} in Table 1).

Fluctuations in the offset of the individual PMT signals affect the measured transverse asymmetry. The mean value and the standard deviation of the PMT signal offsets for all calibration runs (N_{calib}) were calculated and the individual PMT signal offsets were varied to both extremes of their standard deviation. The corresponding changes of the asymmetry caused by the individual PMT signal offset variations were then added. For the final determination of the systematic error (ΔGain in Table 1), the accumulated effect of all offset variations was divided by $\sqrt{N_{\mathrm{calib}}}$ to take into account that the variation represents a statistical fluctuation. The contribution of possible nonlinearities in the asymmetry correction was estimated by excluding 0.1% of the events with the largest absolute correction for each term in Eq. 6, respectively. The absolute values of the resulting changes in the asymmetry were then added up (ΔTails in Table 1).

To identify and correct for possible instrumental asymmetries due to the electronics changing the beam polarity, a half-wave plate in the optical system at the beam source was used to reverse the beam polarity independently of the electronics. To this purpose a similar number of events was acquired for both states of the half-wave plate. Between both states a difference in the measured asymmetry was noticeable. Even though, it was not statistically significant, since the presence of leakage currents in the electronics could not be entirely excluded, the estimated change in the resulting asymmetry for an equal number of events in both states was added to the systematic uncertainty (ΔInversion in Table 1).

In addition, during the XYMO calibration for the measurement on ^{28}Si, an asymmetric average beam profile in vertical direction was identified. In order to estimate the maximum impact of this condition on the result, the XYMO calibration factors were varied from 0 to twice the value obtained in the calibration procedure without changing the correction factors. This led to an additional contribution to the systematic uncertainty (ΔBeamProfile in Table 1).

The resulting transverse asymmetries for ^{28}Si and ^{90}Zr including our recent result for ^{12}C [22] are shown in Fig. 3 together with an extension of the theoretical calculation from Refs. [20,22] to ^{28}Si and ^{90}Zr. The assigned uncertainty of the theoretical prediction

Table 1
Measured beam-normal single spin asymmetries for each spectrometer and kinematical setting. The difference in scattering angle for similar Q^2 values is due to the much wider angular acceptance of spectrometer *A*. Statistical and systematic (individual and total) uncertainty contributions are given in units of parts per million (ppm). The first 5 entries are derived from the asymmetry corrections. ΔCurrentDrop denotes the error from dismissing events with short drops in the beam current. ΔA_I and ΔA_GL correspond to the errors originating in the asymmetry of beam current and gate-length, respectively. ΔGain corresponds to variations of the PMT gain, while ΔTails accounts for possible nonlinearities for large asymmetry corrections. ΔInversion accounts for the different number of events in both states of the half-wave plate. ΔBeamProfile denotes the error associated with an asymmetric beam profile. ΔP corresponds to the error of the polarization measurement.

Target	^{28}Si		^{90}Zr	
Spectrometer	A	B	A	B
Scattering angle	23.51°	19.40°	23.51°	20.67°
Q^2 (GeV$^2/c^2$)	0.038	0.036	0.042	0.042
A_n (ppm)	**−23.302**	**−21.807**	**−17.033**	**−16.787**
$\Delta(\partial\sigma/\partial x)$	0.007	0.003	0.003	0.010
$\Delta(\partial\sigma/\partial y)$	0.013	0.007	0.136	0.131
$\Delta(\partial\sigma/\partial x')$	0.003	0.009	0.054	0.120
$\Delta(\partial\sigma/\partial y')$	0.013	0.014	0.343	0.189
$\Delta(\partial\sigma/\partial E)$	0.099	0.053	0.321	0.259
ΔCurrentDrop	0.006	0.029	0.015	0.031
ΔA_I	0.010	0.010	0.013	0.013
ΔA_GL	0.005	0.005	0.008	0.008
ΔGain	0.067	0.036	0.041	0.018
ΔTails	−0.070	−0.189	+0.108	+0.405
ΔInversion	+0.092	−0.039	−0.406	−0.500
ΔBeamProfile	0.028	0.023	-	-
ΔP	0.210	0.197	0.348	0.343
Total systematic error	+0.553	+0.386	+1.390	+1.527
	−0.531	−0.614	−1.688	−1.622
Statistical error	1.366	1.389	3.524	5.466

comprises contributions related to the Compton slope parameter and terms not enhanced by the large logarithm (see Ref. [20] for details). Both are added in quadrature, since it is expected that they are independent of each other. Since the latter one represents the limitation of the approximation used, 100% uncertainty is assigned to it. The impact on the transverse asymmetry due to the contamination caused by the small fraction of inelastic events in the detector acceptance is considered to be covered by this conservative uncertainty assessment. The error bands in Fig. 3 are then computed by varying the Compton slope parameter by 10% and 20%. For identical kinematics, the theoretical calculation depends only on the mass to charge ratio of the nucleus. Thus, the same asymmetry is expected for both ^{12}C and ^{28}Si.

Within the estimated theoretical uncertainty, the measurements are in agreement with the theoretical prediction. A dramatic disagreement, as it was obtained for ^{208}Pb [21], has not been observed for ^{90}Zr. Though our result is affected by a large statistical uncertainty, its value is not compatible with zero, unlike for the ^{208}Pb measurement. While the mean value of the asymmetry for the zirconium target slightly deviates from the values for the lighter nuclei, the experimental statistical error and the theoretical uncertainty on the Compton slope parameter do not allow for a quantitative statement concerning a clear dependence of A_n on the nuclear charge. The discrepancy to the theoretical prediction seems to be approximately independent on the target nucleus.

The experimental results for the beam-normal single spin asymmetry on ^{28}Si and ^{90}Zr presented in this work contribute significantly to the study of this observable across the nuclear chart from hydrogen to lead. Our results are in agreement with all previous measurements on light and intermediate nuclei confirming that the theoretical model of Ref. [20] correctly grasps the relevant physics. Several explanations for the disagreement with the ^{208}Pb result [21] are conceivable.

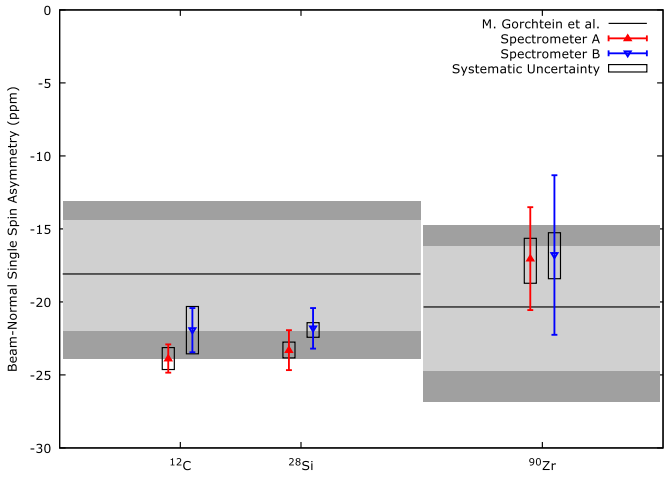

Fig. 3. Extracted transverse asymmetries A_n for ^{12}C (from Ref. [22]), ^{28}Si and ^{90}Zr. The error bars mark the statistical uncertainty and the boxes show the systematic error. The theoretical calculation for $E_\mathrm{b} = 0.570$ GeV and $Q^2 = 0.04$ GeV/c^2 of Ref. [20] (black line) is shown for comparison. The given bands indicate the theoretical error for uncertainties of the Compton slope parameter of 10% (light grey) and 20% (dark grey).

The coefficient C_0 - Eq. (3) - in front of the logarithmically enhanced term could be suppressed for ^{208}Pb. However, this coefficient is fixed by the total photoabsorption cross section, which, to a good approximation, is known to scale with the mass of the nucleus [33] in the relevant energy range. Contributions from nuclear excitations are suppressed as $E_\mathrm{Nucl}/E_\mathrm{beam}$, with E_Nucl a characteristic scale of nuclear excitations (of the order of several MeV).

A possible underestimation of the systematic uncertainty of the theoretical calculation could also explain the observed disagreement. This uncertainty arises from two sources: the term that is not enhanced by the large logarithm was assigned a conservative 100% uncertainty; the Compton form factor has the exponential form, and the respective slope parameter was allowed to vary by 10% - 20%. Given the agreement of the model and the data for all nuclei up to ^{90}Zr, an abrupt change in at least one of these terms is needed to reconcile the calculation with ^{208}Pb.

Eventually, the two-photon approximation used in [20], while appropriate for light and intermediate mass nuclei might be inadequate for heavy nuclei. However, the reasonable agreement of the theory with the ^{90}Zr data (see Fig. 3) as well as a preliminary result of new calculations accounting for Coulomb distortion effects (thus summing corrections $\sim Z\alpha$ to all orders) [34] seem to disprove this explanation.

A new experimental program on Compton scattering at MAMI will permit to reduce the uncertainty of the Compton parameter for intermediate mass nuclei. In addition, measurements of A_n with a ^{12}C target at different beam energies will allow to benchmark the energy dependence of the beam-normal single spin asymmetry in the theoretical treatment. Furthermore, a new measurement of A_n for ^{208}Pb by the PREX-II experiment [35] might provide additional clues to the solution of the current tension.

Declaration of competing interest

The authors declare that they have no known competing financial interests or personal relationships that could have appeared to influence the work reported in this paper.

Acknowledgements

We acknowledge the MAMI accelerator group and all the workshop staff members for outstanding support. This work was sup-

ported by the PRISMA+ (Precision Physics, Fundamental Interactions and Structure of Matter) Cluster of Excellence, the Deutsche Forschungsgemeinschaft through the Collaborative Research Center 1044, and the Federal State of Rhineland-Palatinate. The work of M. Gorchtein was supported by the German-Mexican research collaboration grant No. 278017 (CONACyT) and No. SP 778/4- 1 (DFG), and by the EU Horizon 2020 research and innovation programme, project STRONG- 2020, grant agreement No. 824093.

References

[1] P.L. Anthony, et al., Precision measurement of the weak mixing angle in Møller scattering, Phys. Rev. Lett. 95 (2005) 081601, https://doi.org/10.1103/PhysRevLett.95.081601, arXiv:hep-ex/0504049.
[2] D. Androic, et al., First determination of the weak charge of the proton, Phys. Rev. Lett. 111 (14) (2013) 141803, https://doi.org/10.1103/PhysRevLett.111.141803, arXiv:1307.5275.
[3] D. Androic, et al., Precision measurement of the weak charge of the proton, Nature 557 (7704) (2018) 207–211, https://doi.org/10.1038/s41586-018-0096-0.
[4] F.E. Maas, et al., Measurement of strange quark contributions to the nucleon's form-factors at $Q^2 = 0.230$ (GeV/c)^2, Phys. Rev. Lett. 93 (2004) 022002, https://doi.org/10.1103/PhysRevLett.93.022002, arXiv:nucl-ex/0401019.
[5] D.S. Armstrong, et al., Strange quark contributions to parity-violating asymmetries in the forward G0 electron-proton scattering experiment, Phys. Rev. Lett. 95 (2005) 092001, https://doi.org/10.1103/PhysRevLett.95.092001, arXiv:nucl-ex/0506021.
[6] K.A. Aniol, et al., Constraints on the nucleon strange form-factors at $Q^2 \sim 0.1$ GeV^2, Phys. Lett. B 635 (2006) 275–279, https://doi.org/10.1016/j.physletb.2006.03.011, arXiv:nucl-ex/0506011.
[7] S. Abrahamyan, et al., Measurement of the neutron radius of ^{208}Pb through parity-violation in electron scattering, Phys. Rev. Lett. 108 (2012) 112502, https://doi.org/10.1103/PhysRevLett.108.112502, arXiv:1201.2568.
[8] J. Benesch, et al., The MOLLER experiment: an ultra-precise measurement of the weak mixing angle using Møller scattering, arXiv:1411.4088, 2014.
[9] J. Chen, et al., A white paper on SoLID (Solenoidal Large Intensity Device), arXiv:1409.7741, 2014.
[10] D. Becker, et al., The P2 experiment, Eur. Phys. J. A 54 (11) (2018) 208, https://doi.org/10.1140/epja/i2018-12611-6, arXiv:1802.04759.
[11] M. Gorchtein, C.J. Horowitz, M.J. Ramsey-Musolf, Model-dependence of the γZ dispersion correction to the parity-violating asymmetry in elastic *ep* scattering, Phys. Rev. C 84 (2011) 015502, https://doi.org/10.1103/PhysRevC.84.015502, arXiv:1102.3910.
[12] W.J. Marciano, A. Sirlin, Improved calculation of electroweak radiative corrections and the value of V_{ud}, Phys. Rev. Lett. 96 (2006) 032002, https://doi.org/10.1103/PhysRevLett.96.032002, arXiv:hep-ph/0510099.
[13] A. Afanasev, P.G. Blunden, D. Hasell, B.A. Raue, Two-photon exchange in elastic electron–proton scattering, Prog. Part. Nucl. Phys. 95 (2017) 245–278, https://doi.org/10.1016/j.ppnp.2017.03.004, arXiv:1703.03874.
[14] L. Diaconescu, M.J. Ramsey-Musolf, The vector analyzing power in elastic electron-proton scattering, Phys. Rev. C 70 (2004) 054003, https://doi.org/10.1103/PhysRevC.70.054003, arXiv:nucl-th/0405044.
[15] B. Pasquini, M. Vanderhaeghen, Single spin asymmetries in elastic electron-nucleon scattering, Eur. Phys. J. A 24 (2005) 29–32, https://doi.org/10.1140/epjad/s2005-04-005-3, arXiv:hep-ph/0502144.
[16] B. Pasquini, M. Vanderhaeghen, Resonance estimates for single spin asymmetries in elastic electron-nucleon scattering, Phys. Rev. C 70 (2004) 045206, https://doi.org/10.1103/PhysRevC.70.045206.
[17] A.V. Afanasev, N.P. Merenkov, Large logarithms in the beam normal spin asymmetry of elastic electron-proton scattering, Phys. Rev. D 70 (2004) 073002, https://doi.org/10.1103/PhysRevD.70.073002.
[18] A.V. Afanasev, N.P. Merenkov, Collinear photon exchange in the beam normal polarization asymmetry of elastic electron–proton scattering, Phys. Lett. B 599 (1) (2004) 48–54, https://doi.org/10.1016/j.physletb.2004.08.023, http://www.sciencedirect.com/science/article/pii/S0370269304011700.
[19] E.D. Cooper, C.J. Horowitz, The vector analyzing power in elastic electron-nucleus scattering, Phys. Rev. C 72 (2005) 034602, https://doi.org/10.1103/PhysRevC.72.034602, arXiv:nucl-th/0506034.
[20] M. Gorchtein, C.J. Horowitz, Analyzing power in elastic scattering of the electrons off a spin-0 target, Phys. Rev. C 77 (2008) 044606, https://doi.org/10.1103/PhysRevC.77.044606, arXiv:0801.4575.
[21] S. Abrahamyan, et al., New measurements of the transverse beam asymmetry for elastic electron scattering from selected nuclei, Phys. Rev. Lett. 109 (2012) 192501, https://doi.org/10.1103/PhysRevLett.109.192501, arXiv:1208.6164.
[22] A. Esser, et al., First measurement of the Q^2 dependence of the beam-normal single spin asymmetry for elastic scattering off carbon, Phys. Rev. Lett. 121 (2) (2018) 022503, https://doi.org/10.1103/PhysRevLett.121.022503.
[23] H. Herminghaus, A. Feder, K.H. Kaiser, W. Manz, H. Von Der Schmitt, The design of a cascaded 800-MeV normal conducting CW racetrack microtron, Nucl. Instrum. Methods 138 (1976) 1–12, https://doi.org/10.1016/0029-554X(76)90145-2.
[24] K.I. Blomqvist, et al., The three-spectrometer facility at the Mainz microtron MAMI, Nucl. Instrum. Methods A 403 (1998) 263–301, https://doi.org/10.1016/S0168-9002(97)01133-9.
[25] K. Aulenbacher, et al., The MAMI source of polarized electrons, Nucl. Instrum. Methods A 391 (1997) 498–506, https://doi.org/10.1016/S0168-9002(97)00528-7.
[26] K. Aulenbacher, Polarized beams for electron accelerators, Eur. Phys. J. Spec. Top. 198 (2011) 361–380, https://doi.org/10.1140/epjst/e2011-01499-6.
[27] V. Tioukine, K. Aulenbacher, Operation of the MAMI accelerator with a Wien filter based spin rotation system, Nucl. Instrum. Methods A 568 (2) (2006) 537–542, https://doi.org/10.1016/j.nima.2006.08.022, http://www.sciencedirect.com/science/article/pii/S0168900206014434.
[28] K.H. Steffens, H.G. Andresen, J. Blume-Werry, F. Klein, K. Aulenbacher, E. Reichert, A spin rotator for producing a longitudinally polarized electron beam with MAMI, Nucl. Instrum. Methods A 325 (1993) 378–383, https://doi.org/10.1016/0168-9002(93)90383-S.
[29] A. Tyukin, Master Thesis, Inst. f. Kernphysik, Johannes Gutenberg-Universität Mainz, 2015.
[30] B.S. Schlimme, et al., Vertical beam polarization at MAMI, Nucl. Instrum. Methods A 850 (2017) 54–60, https://doi.org/10.1016/j.nima.2017.01.024, arXiv:1612.02863.
[31] K. Aulenbacher, Helicity correlated asymmetries caused by optical imperfections, Eur. Phys. J. A 32 (2007) 543–547, https://doi.org/10.1140/epja/i2006-10397-8.
[32] M. Seidl, et al., High precision beam energy stabilisation of the Mainz microtron MAMI, in: Proceedings of the 7th European Particle Accelerator Conference, 2000, p. 1930, http://accelconf.web.cern.ch/e00/PAPERS/WEP3B18.pdf.
[33] N. Bianchi, et al., Total hadronic photoabsorption cross section on nuclei in the nucleon resonance region, Phys. Rev. C 54 (1996) 1688–1699, https://doi.org/10.1103/PhysRevC.54.1688.
[34] O. Koshchii, private communication.
[35] K. Paschke, et al., Proposal to Jefferson Lab PAC 38 - Prex-II: precision parity-violating measurement of the neutron skin of lead, https://hallaweb.jlab.org/parity/prex/prexII.pdf.